

1 Meridional distribution of aerosol optical thickness over 2 the tropical Atlantic Ocean

3
4 **P. Kishcha¹, A.M. da Silva², B. Starobinets¹, C.N. Long³, O. Kalashnikova⁴, and**
5 **P. Alpert¹**

6 [1]{Department of Geosciences, Tel-Aviv University, Tel-Aviv, Israel}

7 [2]{Global Modeling and Assimilation Office, NASA/GSFC, Greenbelt, Maryland USA}

8 [3]{Pacific Northwest National Laboratory, Richland, Washington, USA}

9 [4]{Jet Propulsion Laboratory, California Institute of Technology, Pasadena, CA 91109, USA
10 }

11
12 Correspondence to: P. Kishcha (pavelk@post.tau.ac.il)

14 **Abstract**

15 Previous studies showed that, over the global ocean, there is hemispheric asymmetry in
16 aerosols and no noticeable asymmetry in cloud fraction (CF). In the current study, we focus
17 on the tropical Atlantic (30°N – 30°S) which is characterized by significant amounts of
18 Saharan dust dominating other aerosol species over the North Atlantic. We found that, by
19 contrast to the global ocean, over a limited area such as the tropical Atlantic, strong
20 meridional asymmetry in dust aerosols was accompanied by meridional CF asymmetry.
21 During the 10-year study period (July 2002 – June 2012), NASA Aerosol Reanalysis (aka
22 MERRAero) showed that, when the meridional asymmetry in dust aerosol optical thickness
23 (AOT) was the most pronounced (particularly in July), dust AOT averaged separately over the
24 tropical North Atlantic was one order of magnitude higher than dust AOT averaged over the
25 tropical South Atlantic. In the presence of such strong meridional asymmetry in dust AOT in
26 July, CF averaged separately over the tropical North Atlantic exceeded CF averaged over the
27 tropical South Atlantic by 20%. Our study showed significant cloud cover, up to 0.8 – 0.9, in
28 July along the Saharan Air Layer which contributed to above-mentioned meridional CF

1 asymmetry. Both Multi-Angle Imaging SpectroRadiometer (MISR) measurements and
2 MERRAero data were in agreement on seasonal variations in meridional aerosol asymmetry.
3 Meridional asymmetry in total AOT over the Atlantic was the most pronounced between
4 March and July, when dust presence over the North Atlantic was maximal. In September and
5 October, there was no noticeable meridional asymmetry in total AOT and meridional CF
6 distribution over the tropical Atlantic was almost symmetrical.

7

8 **1 Introduction**

9 Satellite observations have been widely used in the study of atmospheric turbidity and aerosol
10 radiative properties because of their capability of providing global coverage on a regular
11 basis. Previous studies, using different space-borne aerosol sensors, discussed the idea that the
12 hemispheres are asymmetric in aerosol distribution (Remer et al., 2008; Kaufman et al.,
13 2005a; Remer and Kaufman, 2006, Mishchenko and Geogdzhayev, 2007, Chou et al., 2002,
14 Zhang and Reid, 2010, Hsu et al., 2012, Kishcha et al, 2007, 2009). The Advanced Very High
15 Resolution Radiometer (AVHRR) satellite data over the ocean were used by Mishchenko and
16 Geogdzhayev (2007) to compare monthly averaged aerosol optical thickness (AOT) over the
17 Northern and Southern Hemispheres. They found a difference in AOT averaged over the two
18 hemispheres. Chou et al. (2002) obtained meridional distribution of AOT over the ocean by
19 using the Sea-viewing Wide Field-of-view Sensor (SeaWiFS) satellite data for the year 1998.
20 Hsu et al. (2012) displayed the asymmetric spatial distribution of seasonally-averaged
21 SeaWiFS AOT from 1997 to 2010. Several studies based on the Moderate Resolution
22 Imaging Spectroradiometer (MODIS) and Multi-Angle Imaging SpectroRadiometer (MISR)
23 data showed that aerosol parameters are distributed asymmetrically on the two hemispheres
24 (Remer et al., 2008; Kaufman et al., 2005a; Remer and Kaufman, 2006, Zhang and Reid,
25 2010, Kishcha et al., 2007, 2009). In our previous study (Kishcha et al., 2009), AOT data
26 from three satellite sensors (MISR, MODIS-Terra, and MODIS-Aqua) were used in order to
27 analyze seasonal variations of meridional AOT asymmetry over the global ocean. The
28 asymmetry was pronounced in the April–July months, while there was no noticeable
29 asymmetry during the season from September to December. Kishcha et al. (2009) mentioned
30 that not only the Northern Hemisphere but also the Southern Hemisphere contributed to the
31 formation of noticeable meridional aerosol asymmetry. During the season of pronounced
32 hemispheric aerosol asymmetry, an increase in AOT was observed over the Northern

1 Hemisphere, while a decrease in AOT was observed over the Southern Hemisphere. It was
2 found that, over the global ocean, there was no noticeable asymmetry in meridional
3 distribution of cloud fraction.

4 Note that the aforementioned studies of AOT asymmetry were based on space-borne remote
5 sensing aerosol measurements. Satellite aerosol data cannot usually distinguish among
6 various aerosol species in the atmosphere. Although some satellite retrievals provide dust
7 fraction of total AOT, there is a discrepancy between satellite datasets due to differences in
8 their assumptions about aerosol and surface properties (Carboni et al., 2012). Consequently,
9 the relative contribution of different aerosol species to hemispheric AOT asymmetry and their
10 effects on meteorological parameters are not well understood.

11 The Sahara desert emits dust in large quantities over the tropical Atlantic (Prospero and
12 Lamb, 2013). Previous studies have shown that desert dust particles can influence the Earth's
13 atmosphere in the following ways: directly by scattering and absorbing solar and thermal
14 radiation, and indirectly by acting as cloud and ice condensation nuclei (Choobari et al, 2013
15 and references therein, Pey et al., 2013). It was shown by Wilcox et al. (2010) that the
16 radiative effect of Saharan dust tends to draw the Atlantic Intertropical Convergence Zone
17 (ITCZ) northward toward the Saharan Air Layer (SAL). Alpert et al. (1998) discussed the
18 response of the atmospheric temperature field to the radiative forcing of Saharan dust over the
19 North Atlantic Ocean. Dust particles over the Atlantic Ocean may essentially influence
20 tropical cloud systems and precipitation (Kaufman et al., 2005b, Min et al., 2009, Ben-Ami et
21 al., 2009, Feingold et al., 2009, Rosenfeld et al., 2001).

22 To our knowledge, over a limited ocean area, meridional asymmetry of aerosols and cloud
23 fraction relative to the equator has not been investigated so far. It was our purpose in the
24 current study to compare meridional asymmetry of aerosols and cloud fraction over the
25 tropical Atlantic (30°N – 30°S) which is characterized by significant amounts of Saharan dust.
26 We determined and compared the contribution of desert dust and that of other aerosol species
27 to aerosol asymmetry between the tropical North and South Atlantic Oceans. Analyzing the
28 meridional distribution of various aerosol species over the tropical Atlantic Ocean was carried
29 out using the NASA Aerosol Reanalysis (aka MERRAero). This reanalysis has been recently
30 developed at NASA's Global Modeling Assimilation Office (GMAO) using a version of the
31 NASA Goddard Earth Observing System-5 (GEOS-5) model radiatively coupled with
32 Goddard Chemistry, Aerosol, Radiation, and Transport (GOCART) aerosols. An important

1 property of GEOS-5 is data assimilation inclusion of bias-corrected aerosol optical thickness
2 from the MODIS sensor on both Terra and Aqua satellites. Of course, AOT assimilation is
3 effective only for two short periods of MODIS's appearance over the study area. All other
4 time (18 hours per day) the GEOS-5 model works independently of MODIS (Kishcha et al.,
5 2014).

6 7 **2 GEOS-5 and the MERRA Aerosol Reanalysis (MERRAero)**

8 GEOS-5 is the latest version of the NASA Global Modeling and Assimilation Office
9 (GMAO) Earth system model, which was used to extend the NASA Modern Era-
10 Retrospective Analysis for Research and Applications (MERRA) with five atmospheric
11 aerosol components (sulfates, organic carbon, black carbon, desert dust, and sea-salt). GEOS-
12 5 includes aerosols based on a version of the Goddard Chemistry, Aerosol, Radiation, and
13 Transport (GOCART) model (Colarco et al., 2010, Chin et al., 2002). Both dust and sea salt
14 have wind-speed dependent emission functions (Colarco et al., 2010), while sulfate and
15 carbonaceous species have emissions principally from fossil fuel combustion, biomass
16 burning, and bio-fuel consumption, with additional biogenic sources of organic carbon.
17 Sulfate has additional chemical production from oxidation of SO₂ and dimethylsulfide
18 (DMS), as well as volcanic SO₂ emissions. Aerosol emissions for sulfate and carbonaceous
19 species are based on the AeroCom version 2 hindcast inventories
20 [<http://aerocom.met.no/emissions.html>]. Daily biomass burning emissions are from the Quick
21 Fire Emission Dataset (QFED) and are derived from MODIS fire radiative power retrievals
22 (Darmenov and da Silva, 2013). GEOS-5 also includes assimilation of AOT observations
23 from the MODIS sensor on both Terra and Aqua satellites. The obtained ten-year (July 2002 –
24 June 2012) MERRA-driven aerosol reanalysis (MERRAero) dataset was applied to the
25 analysis of meridional aerosol asymmetry in the current study. In order to verify the obtained
26 meridional aerosol distribution based on MERRAero, we used the Multi-angle Imaging
27 SpectroRadiometer (MISR) monthly global 0.5° x 0.5° AOT dataset available over the study
28 period.

29 30 **3 Method**

31 Over the tropical Atlantic Ocean (30°N – 30°S), variations of zonal-averaged AOT as a
32 function of latitude were used to analyze meridional aerosol distribution, following our

1 previous study (Kishcha et al., 2009). This included total AOT and AOT of various aerosol
 2 species. To quantify meridional AOT asymmetry, the hemispheric ratio (R) of AOT averaged
 3 separately over the tropical North Atlantic (X_N) to that over the tropical South Atlantic (X_S)
 4 was estimated. The hemispheric ratio is equal to 1 in the case of the two parts of the tropical
 5 Atlantic holding approximately the same averaged AOT, while the ratio is greater (less) than
 6 1 if the North (South) Atlantic dominates the other one. Standard deviation of the reported
 7 hemispheric ratio (Table 1) was estimated in accordance with the following formula by Ku
 8 [1966], NIST/SEMATECH (2006):

$$9 \quad C_R = \frac{1}{\sqrt{N}} \cdot \frac{X_N}{X_S} \cdot \sqrt{\frac{C_N^2}{X_N^2} + \frac{C_S^2}{X_S^2} - 2 \cdot \frac{C_{NS}}{X_N \cdot X_S}}$$

10 where C_N , C_S are standard deviations of zonal averaged AOTs in the tropical North and
 11 South Atlantic Oceans respectively, C_{NS} is their covariance, and $N = 120$ stands for the
 12 number of months in the MISR/ MERRAero AOT monthly data set used.

13 Variations of meridional aerosol distributions were analyzed by using MISR measurements
 14 and MERRAero data during the 10-year period, from July 2002 to June 2012. The MISR
 15 swath width is about 380 km and global coverage is obtained every 9 days. MISR AOT has
 16 been extensively validated against Aerosol Robotic Network (AERONET) Sun photometer
 17 measurements over different regions (Martonchik et al., 2004; Christopher and Wang, 2004;
 18 Kalashnikova and Kahn, 2008; Liu et al., 2004). For the purpose of comparing meridional
 19 distributions of cloud cover with those of AOT during the same 10-year period (July 2002 –
 20 June 2012), Collection 5 of MODIS-Terra Level 3 monthly daytime cloud fraction (CF) data,
 21 with horizontal resolution $1^\circ \times 1^\circ$ was used (King et al., 2003). Furthermore, to analyze
 22 meridional rainfall distribution, the Tropical Rainfall Measuring Mission (TRMM) monthly
 23 $0.25^\circ \times 0.25^\circ$ Rainfall Data Product (3B43 Version 7) was used (Huffman et al., 2007).
 24 MODIS CF data and TRMM data were acquired using the GES-DISC Interactive Online
 25 Visualization and Analysis Infrastructure (Giovanni) as part of NASA Goddard Earth
 26 Sciences (GES) Data and Information Services Center (DISC) (Acker and Leptoukh, 2007).

27

4 Results

4.1 Ocean zone with the predominance of desert dust aerosols

MERRAero showed that the Sahara desert emits a significant amount of dust into the atmosphere over the Atlantic Ocean (Fig. 1, a, c, and e). With respect to different oceans, MERRAero demonstrated that desert dust dominates all other aerosol species only over the Atlantic Ocean. Fig. 1 (b, d, and f) represents spatial distribution of the ratio of dust AOT to AOT of all other aerosol species. The red contour lines represent the boundary of the zone where dust AOT is equal to AOT of all other aerosol species. One can see that, through the 10-year period under consideration, over the Atlantic Ocean within the latitudinal zone between 7°N and 30°N, Saharan dust dominates other aerosol species (Fig. 1b). The longitudinal dimension of this zone is subject to seasonal variability. During the dusty season from March to July, the zone of dust predominance occupies a significant part of the tropical Atlantic between North Africa and Central America. Specifically, as shown in Fig. 1d, in July, the zone of dust predominance is extremely extensive. By contrast, from October to February, this zone is observed only over some limited territory close to North Africa.

Desert dust can be seen not only over the Atlantic Ocean, but also over the Pacific and Indian Oceans (Fig. 1, a, c, and e). However, outside the Atlantic Ocean, one can see only limited zones of desert dust predominance over the Mediterranean Sea and over the Arabian Sea (Fig. 1, b, d, and f). Therefore, the tropical North Atlantic Ocean is the largest ocean area where dust particles determine the atmospheric aerosol content, based on MERRAero data.

4.2 Meridional distribution of total AOT over the tropical Atlantic Ocean

Figure 2a represents meridional distribution of ten-year mean AOT (July 2002 – June 2012), zonal averaged over the tropical Atlantic Ocean. One can see that MERRAero showed similarity to the meridional AOT distribution, based on MISR data (Fig. 2a). Specifically, MERRAero was able to reproduce the meridional asymmetry in the AOT distribution, including a monomodal maximum in the tropical North Atlantic and a minimum in the tropical South Atlantic. This monomodal AOT maximum was discussed in our previous study (Kishcha et al., 2009). Both MISR and MERRAero showed that, in the minimum, the AOT values were three times lower than those in the maximum. We quantified meridional AOT asymmetry in the tropical Atlantic Ocean (30°N – 30°S) by obtaining the hemispheric ratio (R_{AOT}) of AOT averaged separately over the tropical North Atlantic to AOT averaged over

1 the tropical South Atlantic: R_{AOT} was estimated to be about 1.7 (Table 1). This means that,
2 over the 10-year period under consideration, there were much more aerosol particles over the
3 tropical North Atlantic than over the tropical South Atlantic.

4 5 **4.3 Seasonal variations of meridional distribution of AOT**

6 For each month of the year, we analyzed variations of meridional distribution of AOT over
7 the tropical Atlantic Ocean (Fig. 3). It was found that the meridional AOT distribution is
8 seasonal dependent. In particular, both MISR and MERRAero were in agreement that the
9 monomodal AOT maximum, a characteristic feature of meridional asymmetry in AOT, exists
10 but not in each month. In the months from September to October, two AOT maxima can be
11 observed: one maximum in the North Atlantic, and another one in the South Atlantic.

12 Fig. 4 represents month-to-month variations of the hemispheric ratio R_{AOT} over the tropical
13 Atlantic for each month of the year. Both MISR and MERRAero showed that meridional
14 AOT asymmetry was most pronounced during the season from March to July. One can see
15 that, from month to month during the year, R_{AOT} ranges from 1 to 2.4, while during the season
16 of pronounced meridional aerosol asymmetry (March – July) R_{AOT} ranges from 2.0 – 2.4. In
17 September and October, R_{AOT} was close to 1, indicating no noticeable asymmetry (Fig. 4).

18 19 **4.4 Meridional distribution of AOT of various aerosol species**

20 Fig. 2c represents meridional distribution of ten-year mean MERRAero AOT for total AOT
21 (Total), dust AOT (DU), organic and black carbon aerosol AOT (OC & BC), and AOT of
22 other aerosol species (Other), zonal averaged over the tropical Atlantic Ocean. One can see
23 that meridional dust distribution is much more asymmetric relative to the equator than
24 meridional distribution of OC & BC and other aerosol species. The meridional asymmetry of
25 DU, characterized by the hemispheric ratio (R_{DU}) of dust AOT was about 11 (Table 2). Such
26 strong asymmetry in meridional distribution of desert dust over the ocean can be explained by
27 its transport by winds from the Sahara desert to the ocean in the North Atlantic. Being the
28 major contributor to the AOT maximum in the North Atlantic, Saharan dust was responsible
29 for the pronounced meridional AOT asymmetry in total AOT over the tropical Atlantic
30 Ocean. Carbon aerosols also displayed some meridional asymmetry characterized by the
31 hemispheric ratio $R_{OC\&BC} = 0.7$, although this asymmetry was much less pronounced than that
32 of desert dust (Fig. 2c and Table 2). Meridional distribution of AOT of other aerosol species

1 was almost symmetrical (R_{Other} is 1.1) (Table 2). Therefore, aerosols over the tropical Atlantic
2 can be divided into two groups with different meridional distribution relative to the equator:
3 dust and carbonaceous aerosols were distributed asymmetrically, while other aerosol species
4 were distributed almost symmetrically.

5 MERRAero showed that seasonal variations of transatlantic Saharan dust transport
6 determined the seasonal variations of meridional dust asymmetry. In May - July, when
7 meridional asymmetry in dust AOT over the tropical North Atlantic was the most
8 pronounced, dust AOT averaged separately over the tropical North Atlantic was one order of
9 magnitude higher than dust AOT averaged over the tropical South Atlantic (Table 2). In July,
10 the most pronounced meridional asymmetry of dust AOT was characterized by the
11 hemispheric ratio R_{DU} of about 30 (Table 2).

12 When dust presence over the North Atlantic was minimal, the contribution of other aerosol
13 species to the meridional distribution of total AOT could be significant. In particular, in
14 December, the maximum in OC & BC at low-latitudes (due to the transport of bio-mass
15 burning smoke) contributed significantly to the maximum in total AOT in the tropical North
16 Atlantic (Fig. 5a). Note that the reason for the aforementioned transport of bio-mass burning
17 aerosols is the burning of agricultural waste in the Sahelian region of northern Africa. This
18 burning activity is maximal during December – February (Haywood et al., 2008). MERRAero
19 showed that no noticeable meridional asymmetry of total AOT was observed in September
20 and October (Fig. 4). This is because the contribution of carbonaceous aerosols (OC & BC) to
21 total AOT over the South Atlantic is approximately equal to the contribution of Saharan dust
22 to total AOT in the North Atlantic (Fig. 5). The reason for the observed increase in OC & BC
23 over the South Atlantic in September and October is that these months fall within the burning
24 period in Central Africa, where slash-and-burn agriculture is prevalent (Tereszchuk et al.,
25 2011). In September and October, AOT of carbonaceous aerosols over the tropical South
26 Atlantic was five times higher than that over the tropical North Atlantic ($R_{\text{OC\&BC}} = 0.2$) (Table
27 2).

28 By contrast to dust and carbonaceous aerosols, meridional distribution of AOT of other
29 aerosol species remains almost symmetrical through out all months (the hemispheric ratio
30 R_{Other} ranged from 1.0 – 1.3) (Table 2). This group includes marine aerosols, such as sea-salt
31 and dimethylsulfide (DMS) aerosols, which are produced everywhere in the tropical Atlantic

1 Ocean. This is the reason why their meridional distribution, zonal averaged over the ocean, is
2 almost symmetrical relative to the equator.

4 **4.5 Meridional distribution of cloud fraction**

5 We analyzed meridional distribution of cloud cover over the tropical (30°N – 30°S) Atlantic
6 Ocean, which includes the area of transatlantic Saharan dust transport within SAL. Fig. 2b
7 represents the meridional distribution of 10-year mean cloud fraction, zonal averaged over the
8 Atlantic Ocean. One can see the local maximum near the equator due to clouds concentrated
9 over the Intertropical Convergence Zone: this maximum shifts to the north from the equator.
10 Despite this CF maximum, the hemispheric CF ratio (R_{CF}), characterized by the ratio of CF
11 averaged separately over the tropical North and over the South Atlantic, did not exceed 1.1
12 (Table 1).

13 As mentioned in Sect. 4.4, MERRAero showed that dust and carbonaceous aerosols were
14 distributed asymmetrically in relation to the equator, while other aerosol species were
15 distributed almost symmetrically. During the period of pronounced meridional AOT
16 asymmetry over the tropical Atlantic from May - July, dust AOT averaged separately over the
17 tropical North Atlantic was about one order of magnitude higher than dust AOT averaged
18 over the tropical South Atlantic (Table 2). In July, the hemispheric ratio R_{DU} was roughly 30.
19 In the presence of such strong meridional dust asymmetry, in July, R_{CF} reached 1.2 (Table 2).
20 As shown in previous study (Kishcha et al., 2009), over the global ocean, R_{AOT} was about 1.5,
21 while R_{CF} was 1. Therefore, by contrast to the global ocean (where meridional CF distribution
22 was symmetrical over the two hemispheres), over the tropical Atlantic in July, CF averaged
23 separately over the tropical North Atlantic exceeded CF averaged over the tropical South
24 Atlantic by 20%. In September – October, when total AOT was almost symmetrical over the
25 tropical Atlantic (R_{AOT} was close to 1), meridional CF distribution was also almost
26 symmetrical (R_{CF} was equal to 1, (Table 2)).

27 Fig. 6 represents meridional distribution of MODIS CF and TRMM accumulated rainfall,
28 zonal averaged over the tropical Atlantic Ocean, for all months of the year. One can see some
29 changes in CF from month to month on the high background level of approximately 0.6. This
30 background level of CF is almost the same over the tropical North and South Atlantic Oceans.

31 In each month, the main CF maximum coincides with the Atlantic Ocean inter-tropical
32 convergence zone, which is characterized by intensive rainfall (Fig. 6). In the summer months

1 (when pronounced meridional dust asymmetry was observed), MODIS CF data showed
2 significant CF to the north from the main CF maximum, over the latitudes of transatlantic dust
3 transport within the Saharan Air Layer (SAL) (Fig. 6, g to i). Saharan dust travels across the
4 Atlantic Ocean within the hot and dry Saharan Air Layer (Dunion and Velden, 2004). The
5 SAL's base is at ~900 – 1800 m and the top is usually below 5500 m (Diaz et al., 1976). The
6 significant cloud fraction along SAL, together with the Atlantic Inter-tropical Convergence
7 Zone (centered over the tropical North Atlantic) contributed to the above-mentioned
8 meridional CF asymmetry. Following is our analysis of cloud fraction in the area of the
9 Saharan Air Layer in July, when the most pronounced meridional dust asymmetry was
10 observed.

11

12 **4.5.1 Cloud fraction in the area of the Saharan Air Layer in July**

13 Figure 7 represents meridional distribution of the 10-year mean of MERRAero dust AOT,
14 MODIS-Terra cloud fraction, and TRMM accumulated rainfall, zonal averaged over the
15 Atlantic Ocean (60°W – 0°E). The near-equatorial maximum in meridional distribution of
16 TRMM accumulated rainfall indicates the position of the North Atlantic Ocean inter-tropical
17 convergence zone (ITCZ) (Fig. 7). One can see that, in July, when dust presence over the
18 Atlantic is maximal, the meridional distribution of CF becomes essentially asymmetric with
19 respect to the center of ITCZ. In particular, significant CF up to 0.8 is seen northward from
20 ITCZ, over the latitudes with SAL presence (12°N – 24°N) (Fig. 7). These values are higher
21 than the 10-year mean MODIS CF over the tropical North Atlantic (0.66) (Table 1). One can
22 consider that, in the North Atlantic, the wide maximum in the meridional distribution of CF
23 consists of two different partly-overlapping maxima: one CF maximum located within ITCZ,
24 and the other CF maximum located over the ocean area where Saharan dust is transported
25 within the SAL across the Atlantic (Fig. 7).

26 More detailed information about the aforementioned two partly-overlapping maxima in the
27 meridional distribution of CF in July can be obtained from a comparison between spatial
28 distribution of ten-year mean MERRAero dust AOT and MODIS CF over the tropical North
29 Atlantic (Fig. 8, a and b). It is clearly seen that the ocean area with Saharan dust transported
30 across the Atlantic is covered by cloudiness characterized by significant values of MODIS CF
31 up to 0.8 – 0.9. This CF is higher than the 10-year mean MODIS CF over the tropical North
32 Atlantic (0.66) (Table 1). Note that there is a strong difference between the two zones of

1 significant CF in the North Atlantic. High values of CF within ITCZ are accompanied by
2 intensive rainfall (Fig. 8, b and c). By contrast, the area of SAL with significant CF (12°N –
3 24°N) is characterized by essentially lower precipitation (Fig. 8, b and c).

4 We analyzed the 10-year mean (July 2002 – June 2012) of dust and cloudiness over six zones,
5 each 6° x 6°, located along the area of transatlantic dust transport (Fig. 8a). In July, there was
6 a decline of approximately 300% in dust AOT from zone 1 to zone 6 (Fig. 9a). The reason for
7 the decline in dust AOT with increasing distance from dust sources in the Sahara is
8 gravitational settling of dust particles (mainly coarse fraction). Zone-to-zone variations of
9 MODIS CF were considerably less pronounced: CF over zones 1 and 2 ranged from 0.8 – 0.9,
10 while CF over zones from 3 to 6 was about 0.7 (Fig. 9b). Zone-to-zone variations of 10-year
11 mean TRMM accumulated rainfall revealed a significant increase over zones remote from the
12 Sahara: there were higher values (70 mm – 110 mm) over zones 5 and 6 than over zones 1 to
13 4 (20 mm – 30 mm) (Fig. 9b). This increase in rainfall over zones 5 and 6 indicated an
14 increase in the precipitation ability of clouds over these zones.

15 Temperature inversion at the base of the Saharan Air Layer prevents deep cloud development
16 and precipitation (Prospero and Carlson, 1972). We analyzed temperature inversion over
17 zones 1 to 6. Fig. 10 represents vertical profiles of atmospheric temperature averaged over the
18 specified zones, in July during the 10-year period under consideration. The observed
19 temperature inversion over zones 1 to 4 (Fig. 10) prevented convective activity and
20 precipitation, which explains the observed low accumulated rainfall (Fig. 9b). There was no
21 temperature inversion over zones 5 and 6 (Fig. 10). In the absence of temperature inversion
22 there is no suppression of deep cloud formation and precipitation. This explains the increase
23 in TRMM accumulated rainfall over zones 5 and 6.

24

25 **5 Conclusions**

26 Meridional distribution of aerosol optical thickness and cloud fraction were analyzed using
27 10-year satellite measurements from MISR and MODIS, together with MERRAero data (July
28 2002 – June 2012).

29 In accordance with our previous study (Kishcha et al., 2009), over the global ocean, there is
30 hemispheric asymmetry in aerosols and no noticeable asymmetry in cloud fraction. In the
31 current study, we focus on the tropical Atlantic (30°N – 30°S) which is characterized by

1 significant amounts of Saharan dust. We found that, by contrast to the global ocean, over a
2 limited area such as the tropical Atlantic, strong meridional asymmetry in dust aerosols was
3 accompanied by meridional CF asymmetry.

4 When meridional AOT asymmetry over the tropical North Atlantic was the most pronounced,
5 dust AOT averaged separately over the tropical North Atlantic was one order of magnitude
6 higher than dust AOT averaged over the tropical South Atlantic. In July, the most pronounced
7 meridional asymmetry of dust AOT was characterized by the hemispheric ratio R_{DU} of
8 approximately 30. In the presence of such strong meridional asymmetry in dust AOT in the
9 summer months, CF averaged separately over the tropical North Atlantic exceeded CF
10 averaged over the tropical South Atlantic by 20%. Our study showed that, in July, significant
11 cloud cover (up to 0.8 – 0.9) with limited precipitation ability (TRMM accumulated rainfall
12 20-30 mm/month) was observed along the Saharan Air Layer. These CF values are higher
13 than the 10-year mean MODIS CF over the tropical North Atlantic (0.66) (Table 1). This
14 significant cloud fraction along SAL together with the Atlantic Inter-tropical Convergence
15 Zone (centered over the tropical North Atlantic and characterized by significant cloud cover)
16 contribute to the above-mentioned meridional CF asymmetry.

17 With respect to different oceans, only over the Atlantic Ocean did MERRAero demonstrate
18 that desert dust dominated all other aerosol species and was responsible for meridional
19 aerosol asymmetry there. MERRAero showed that, over the tropical Atlantic, dust and
20 carbonaceous aerosols were distributed asymmetrically relative to the equator, while other
21 aerosol species were distributed almost symmetrically.

22 Both MISR measurements and MERRAero data were in agreement on seasonal variations in
23 meridional aerosol asymmetry. Meridional asymmetry in total AOT over the Atlantic was the
24 most pronounced between March and July, when dust presence over the North Atlantic was
25 maximal. In September and October, there was no noticeable meridional aerosol asymmetry
26 in total AOT (R_{AOT} was close to 1). During these two months, the contribution of
27 carbonaceous aerosols to total AOT in the South Atlantic was comparable to the contribution
28 of dust aerosols to total AOT in the North Atlantic. Our study showed that, in September and
29 October, meridional CF distribution over the tropical Atlantic was almost symmetrical (R_{CF}
30 was close to 1).

31

1 **Acknowledgements**

2 We acknowledge the GES-DISC Interactive Online Visualization and Analysis Infrastructure
3 (Giovanni) for providing us with MODIS CF and TRMM data. Dr. Long acknowledges
4 support from the Office of Biological and Environmental Research of the U.S. Department of
5 Energy as part of the Atmospheric Systems Research Program. The Tel-Aviv University team
6 acknowledges support from the international Virtual Institute DESERVE (Dead Sea Research
7 Venue), funded by the German Helmholtz Association.

8

9

1 **References**

- 2 Acker, J.G., and Leptoukh, G.: Online analysis enhances use of NASA Earth science data,
3 Eos Trans. AGU, 88(2), doi:10.1029/2007EO020003, 2007.
- 4 Alpert, P., Kaufman, Y.J., Shay-El, Y., Tanre, D., da Silva, A., Schubert, S., and Joseph, J.H.:
5 Quantification of dust-forced heating of the lower troposphere. *Nature* 395, 367-370, 1998.
- 6 Ben-Ami, Y., Koren, I., and Altaratz, O.: Patterns of North African dust transport over the
7 Atlantic: winter vs. summer, based on CALIPSO first year data. *Atmos. Chem. Phys.*, 9,
8 7867–7875, 2009.
- 9 Carboni, E., Thomas, G., Sayer, A, et al.: Intercomparison of desert dust optical depth from
10 satellite measurements. *Atmos. Meas. Tech.*, 5,1973-2002, doi:10.5194/amt-5-1973-2012,
11 2012.
- 12 Chin, M., Ginoux, P., Kinne, S., Torres, O., Holben, B., Duncan, B.N., Martin, R.V., Logan,
13 J., Higurashi, A., Nakajima, T.: Tropospheric aerosol optical thickness from the GOCART
14 model and comparisons with satellite and sun photometer measurements. *J. Atmos. Phys.* 59,
15 461–483, doi: [http://dx.doi.org/10.1175/1520-0469\(2002\)059](http://dx.doi.org/10.1175/1520-0469(2002)059), 2002.
- 16 Colarco, P., da Silva, A., Chin, M., and Diehl, T.: Online simulations of global aerosol
17 distributions in the NASA GEOS-4 model and comparisons to datellite and ground-based
18 aerosol optical depth. *J. Geophys. Res.*, 115, D14207, doi:10.1029/2009JD012820, 2010.
- 19 Choobari, O.A., Zawar-Reza, P., and Sturman, A.: The global distribution of mineral dust and
20 its impacts on the climate system: A review. *Atmospheric Research*, 138, 152-165,
21 <http://dx.doi.org/10.1016/j.atmosres.2013.11.007>, 2014.
- 22 Chou, M.-D., Chan, P.-K and Wang, M.: Aerosol radiative forcing derived from SeaWIFS-
23 Retrieved aerosol optical properties. *J. Atmos. Sci.* (Global Aerosol Climatology special
24 issue), 59, 748-757, 2002.
- 25 Christopher, S., and Wang, J.: Intercomparison between multi-angle Imaging
26 SpectroRadiometer (MISR) and sunphotometer aerosol optical thickness in dust source
27 regions of China, implications for satellite aerosol retrievals and radiative forcing
28 calculations. *Tellus B*, 56, 451–456, 2004.

1 Darnenov, A., and da Silva, A.: The quick fire emissions dataset (QFED) - Documentation of
2 versions 2.1, 2.2 and 2.4. NASA Technical Report Series on Global Modeling and Data
3 Assimilation. NASA TM-2013-104606, 32, 183p, 2013.

4 Diaz, H.F., Carlson, T.N., and Prospero, J.M.: A study of the structure and dynamics of the
5 Saharan air layer over the northern equatorial Atlantic during BOMEX, NOAA Tech Memo
6 ERL WMPO-32, 61 pp., NOAA, Silver Spring, Md., 1976.

7 Dunion, J.P., and Velden, C.S.: The impact of the Saharan air layer on Atlantic tropical
8 cyclone activity, *Bull. Am. Meteorol. Soc.*, 85(3), 353– 365, doi:10.1175/BAMS-85-3-353,
9 2004.

10 Feingold, G., Cotton, W., Lohmann, U., and Levin, Z.: Effects of pollution aerosols and
11 biomass burning on clouds and precipitation: numerical modeling studies. In *Aerosol
12 pollution impact on precipitation*. Eds.: Z. Leven and W. Cotton. Springer, Chapter 7, 243 –
13 278, 2009.

14 Haywood, J.M., Pelon, J., Formenti, P., et al.: Overview of the Dust and Biomass-burning
15 Experiment and African Monsoon Multidisciplinary Analysis Special Observing Period-0. *J.
16 Geophys. Res.*, 113, D00C17, doi:10.1029/2008JD010077, 2008.

17 Hsu, N.C., Gautam, R., Sayer, A.M., Bettenhausen, C., Li, C., Jeong, M.J., Tsay, S.C., and
18 Holben, B.: Global and regional trends of aerosol optical depth over land and ocean using
19 SeaWiFS measurements from 1997 to 2010. *Atmos. Chem. Phys. Discuss.*, 12, 8465-8501,
20 doi:10.5194/acpd-12-8465-2012, 2012.

21 Huffman, G.J., Adler, R.F., Bolvin, D.T., Gu, G., Nelkin, E.J., Bowman, K.P., Hong, Y.,
22 Stocker, E.F., Wolff, D.B.: The TRMM multisatellite precipitation analysis (TMPA): quasi-
23 global, multiyear, combined-sensor precipitation estimates at fine scales. *J.
24 Hydrometeorology*, 8, 38 – 55, doi: 10.1175/JHM560.1, 2007.

25 Kalashnikova, O.V. and Kahn, R.: Mineral dust plume evolution over the Atlantic from MISR
26 and MODIS aerosol retrievals. *J. Geophys. Res.*, 113, D24204, doi:10.1029/2008JD010083,
27 2008.

28 Kaufman, Y.J., Boucher, O., Tanre, D., Chin, M., Remer, L.A. and Takemura, T.: Aerosol
29 anthropogenic component estimated from satellite data, *Geophys. Res. Lett.*, 32, L17804,
30 doi:10.1029/2005GL023125, 2005a.

1 Kaufman, Y.J., Koren, I., Remer, L., Rosenfeld, D., and Rudich, Y.: The effect of smoke,
2 dust, and pollution aerosol on shallow cloud development over the Atlantic Ocean. *Proc. Natl.*
3 *Acad. Sci. U.S.A.*, 102, 11,207-11,212, 2005b.

4 King, M.D., Menzel, W.P., Kaufman, Y.J., Tanre, D., Gao, B.C., Platnick, S., Ackerman,
5 S.A., Remer, L.A., Pincus, R. and Hubanks, P.A.: Cloud and aerosol properties, precipitable
6 water, and profiles of temperature and humidity from MODIS. *IEEE Transactions on*
7 *Geoscience and Remote Sensing*, 41(2), 442-458, 2003.

8 Kishcha, P., Starobinets, B., and Alpert, P.: Latitudinal variations of cloud and aerosol optical
9 thickness trends based on MODIS satellite data. *Geophys. Res. Lett.*, 34, L05810,
10 doi:10.1029/2006GL028796, 2007.

11 Kishcha, P., Starobinets, B., Kalashnikova, O., Long, C.N., and Alpert, P.: Variations in
12 meridional aerosol distribution and solar dimming. *J. Geophys. Res.*, 114, D00D14,
13 doi:10.1029/2008JD010975, 2009.

14 Kishcha, P., da Silva, A.M., Starobinets, B., and Alpert, P.: Air pollution over the Ganges
15 basin and north-west Bay of Bengal in the early post-monsoon season based on NASA
16 MERRAero data. *J. Geophys. Res. Atmos.*, 119, doi:10.1002/2013JD020328, 2014.

17 Ku, H.: Notes on the use of propagation of error formulas. *J. Research of National Bureau of*
18 *Standards – C. Engineering and Instrumentation*, 70C, No.4, 263-273, 1966.

19 Liu, Y., Sarnat, J.A., Coull, B.A., Koutrakis, P. and Jacob, D.J.: Validation of Multiangle
20 Imaging Spectroradiometer (MISR) aerosol optical thickness measurements using Aerosol
21 Robotic Network (AERONET) observations over the contiguous United States. *J. Geophys.*
22 *Res.*, 109, D06205, doi:10.1029/2003JD003981, 2004.

23 Min, Q.I., Li, R., Lin, B., Joseph, F., Wang, S., Hu, Y., Morris, V., and Chang, F.: Evidence
24 of mineral dust altering cloud microphysics and precipitation. *Atmos. Chem. Phys.*, 9, 3223-
25 3231, doi:10.5194/acp-9-3223-2009, 2009.

26 Matronchik, J.V., Diner, D.J., Kahn, R., and Gaitley, B.: Comparison of MISR and
27 AERONET aerosol optical depths over desert sites. *Geophys. Res. Lett.*, 31, L16102,
28 doi:10.1029/2004GL019807, 2004.

29 Mishchenko, M.I., and Geogdzhayev, I.V.: Satellite remote sensing reveals regional
30 tropospheric aerosol trends. *Opt. Express*, 15, 7423 – 7438, doi:10.1364/OE.15.007423, 2007.

1 NIST/SEMATECH e-Handbook of Statistical Methods: 2006.
2 <http://www.itl.nist.gov/div898/handbook/>.

3 Pey, J., Querol, X., Alastuey, A., Forastiere, F., and Stafoggia, M.: African dust outbreaks
4 over the Mediterranean Basin during 2001–2011: PM10 concentrations, phenomenology and
5 trends, and its relation with synoptic and mesoscale meteorology. *Atmos. Chem. Phys.*, 13,
6 1395–1410, doi:10.5194/acp-13-1395-2013, 2013.

7 Prospero, J., and Carlson, T.: Vertical and areal distribution of Saharan dust over the Western
8 Equatorial North Atlantic Ocean. *J. Geophys. Res.*, 77, 5255 – 5265,
9 doi:10.1029/JC077i027p05255, 1972.

10 Prospero, J., and Lamb, J.: African droughts and dust transport to the Caribbean: climate
11 change and implications. *Science*, 302, 1024-1027, doi:10.1126/science.1089915, 2003.

12 Remer, L.A. and Kaufman, Y.J.: Aerosol direct radiative effect at the top of the atmosphere
13 over cloud free ocean derived from four years of MODIS data. *Atmos. Chem. Phys.*, 6, 237-
14 253, 2006.

15 Remer, L.A., Kleidman, R.G., Levy, R.C., Kaufman, Y.J., Tanre, D., Mattoo, S., Martins,
16 J.V., Ichoku, C., Koren, I., Hongbin, Yu, Holben, B.N.: Global aerosol climatology from the
17 MODIS satellite sensors. *J. Geophys. Res.*, 113, D14S07, doi:10.1029/2007JD009661, 2008.

18 Rosenfeld, D., Rudich, Y., Lahav, R.: Desert dust suppressing precipitation - a possible
19 desertification feedback loop. *Proceedings of the National Academy of Sciences*, 98, 5975-
20 5980, 2001.

21 Tereszchuk, K.A., Gonz´alez Abad1, G., Clerbaux, C., Hurtmans, D., Coheur, P.F., and P.F.
22 Bernath, P.F.: ACE-FTS measurements of trace species in the characterization of biomass
23 burning plumes. *Atmos. Chem. Phys.*, 11, 12169–12179, doi:10.5194/acp-11-12169-2011,
24 2011.

25 Wilcox, E.M., Lau, K.M., and Kim, K.M.: A northward shift of the North Atlantic Ocean
26 Intertropical Convergence Zone in response to summertime Saharan dust outbreaks, *Geophys.*
27 *Res. Lett.*, 37, L04804, doi:10.1029/2009GL041774, 2010.

28 Zhang, J.L. and Reid, J.S.: A decadal regional and global trend analysis of the aerosol optical
29 depth using a data-assimilation grade over-water MODIS and Level 2 MISR aerosol products.
30 *Atmos. Chem. Phys.*, 10, 10949-10963, doi:10.5194/acp-10-10949-2010, 2010.

31

1 Table 1. Average AOT and CF over the tropical North (X_N) and South (X_S) Atlantic and their
2 hemispheric ratio (R)^a . 10-year MERRAero AOT, MISR AOT, and MODIS CF data were
3 used.

Data set	$X_N \pm \sigma_N$	$X_S \pm \sigma_S$	$R \pm \sigma_R$
MISR AOT	0.25 ± 0.06	0.15 ± 0.05	1.70 ± 0.06
MERRAero AOT	0.19 ± 0.05	0.12 ± 0.05	1.61 ± 0.06
MODIS CF	0.66 ± 0.09	0.61 ± 0.06	1.08 ± 0.01

4 ^aStandard deviations of X_N , X_S , and R are designated by σ_N , σ_S , σ_R respectively.

5

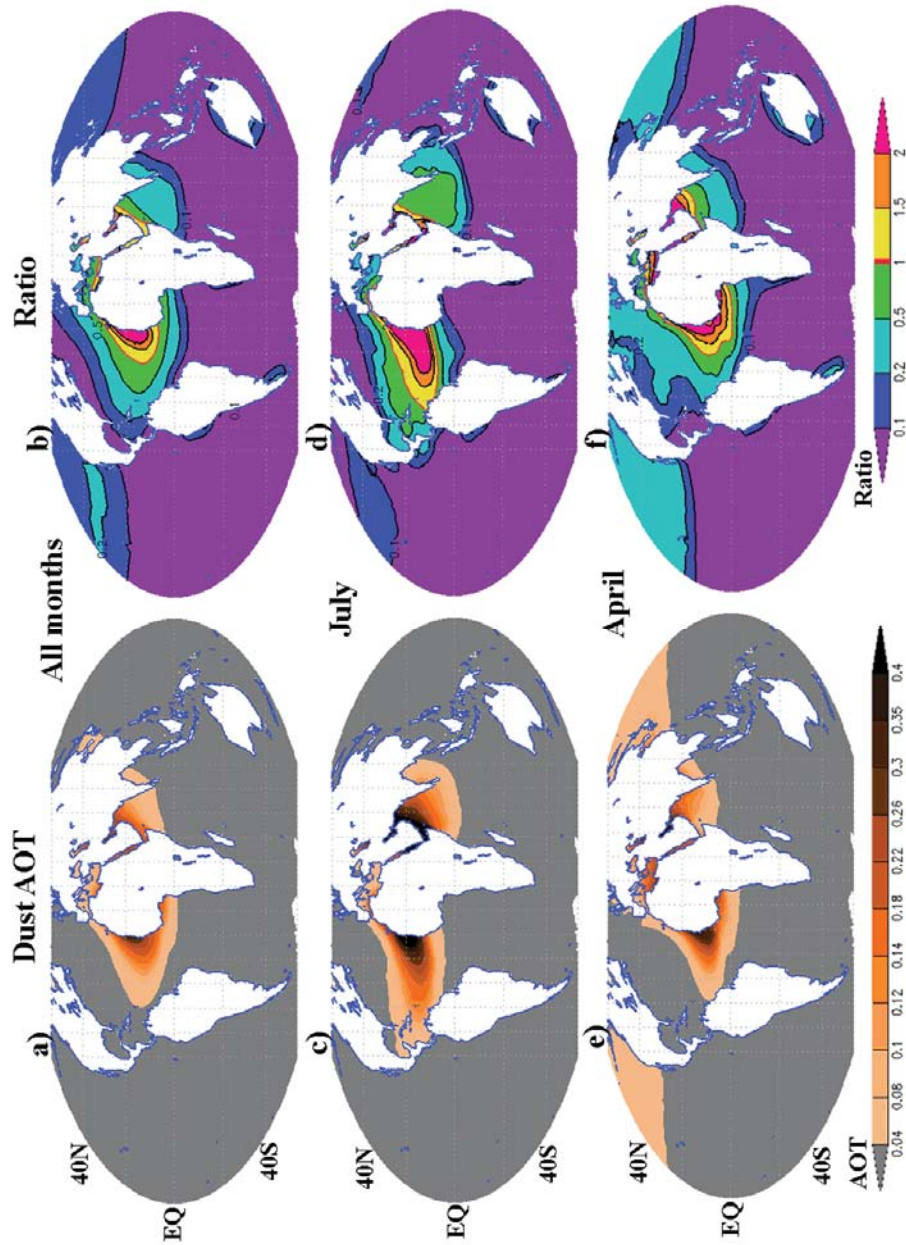
1 Table 2. The hemispheric ratio (\pm standard deviation) of dust AOT (DU), organic and black
 2 carbon AOT (OC & BC), other aerosol species AOT (Other), and MODIS CF over the
 3 tropical Atlantic Ocean (30°N – 30°S). 10-year MERRAero data and MODIS CF data were
 4 used.

Month	DU	OC & BC	Other	MODIS CF
All months	11.50 \pm 1.20	0.70 \pm 0.10	1.10 \pm 0.10	1.08 \pm 0.01
January	6.10 \pm 2.30	1.30 \pm 0.50	1.10 \pm 0.10	1.10 \pm 0.07
February	4.20 \pm 1.80	1.20 \pm 0.40	1.20 \pm 0.10	1.15 \pm 0.09
March	6.90 \pm 3.20	2.00 \pm 0.40	1.20 \pm 0.10	1.14 \pm 0.10
April	8.80 \pm 4.10	2.70 \pm 0.40	1.20 \pm 0.10	1.07 \pm 0.09
May	21.00 \pm 10.10	1.70 \pm 0.30	1.20 \pm 0.10	1.14 \pm 0.07
June	23.50 \pm 10.80	0.90 \pm 0.30	1.30 \pm 0.10	1.20 \pm 0.09
July	29.30 \pm 10.30	0.70 \pm 0.30	1.30 \pm 0.20	1.21 \pm 0.08
August	25.00 \pm 8.50	0.40 \pm 0.10	1.10 \pm 0.10	1.04 \pm 0.07
September	23.80 \pm 6.70	0.20 \pm 0.10	0.90 \pm 0.10	0.98 \pm 0.05
October	17.00 \pm 4.30	0.20 \pm 0.10	0.80 \pm 0.10	0.97 \pm 0.05
November	9.70 \pm 2.30	0.70 \pm 0.20	0.80 \pm 0.10	0.98 \pm 0.05
December	6.80 \pm 1.90	1.00 \pm 0.30	0.90 \pm 0.10	1.05 \pm 0.05

5

6

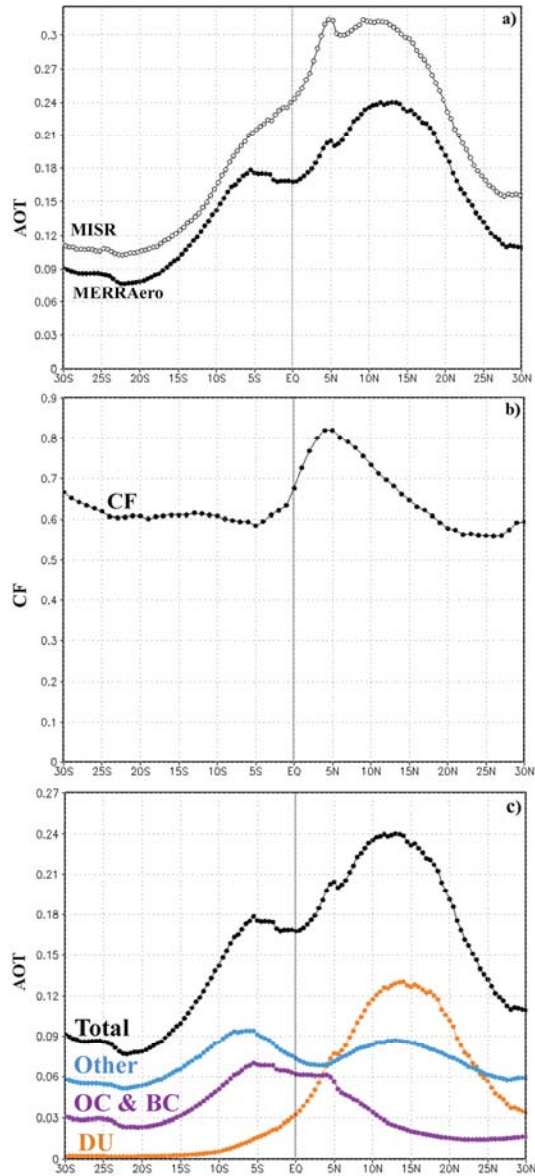
7



2 Figure 1. Spatial distributions of (a, c, and e) dust AOT (DU) and (b, d, and f) the ratio of DU
 3 to AOT of all other aerosol species, based on the 10-y MERRAero data. In the right panel, the
 4 red contour line represents the boundary of the zone where dust AOT is equal to AOT of all
 5 other aerosol species.

6
 7

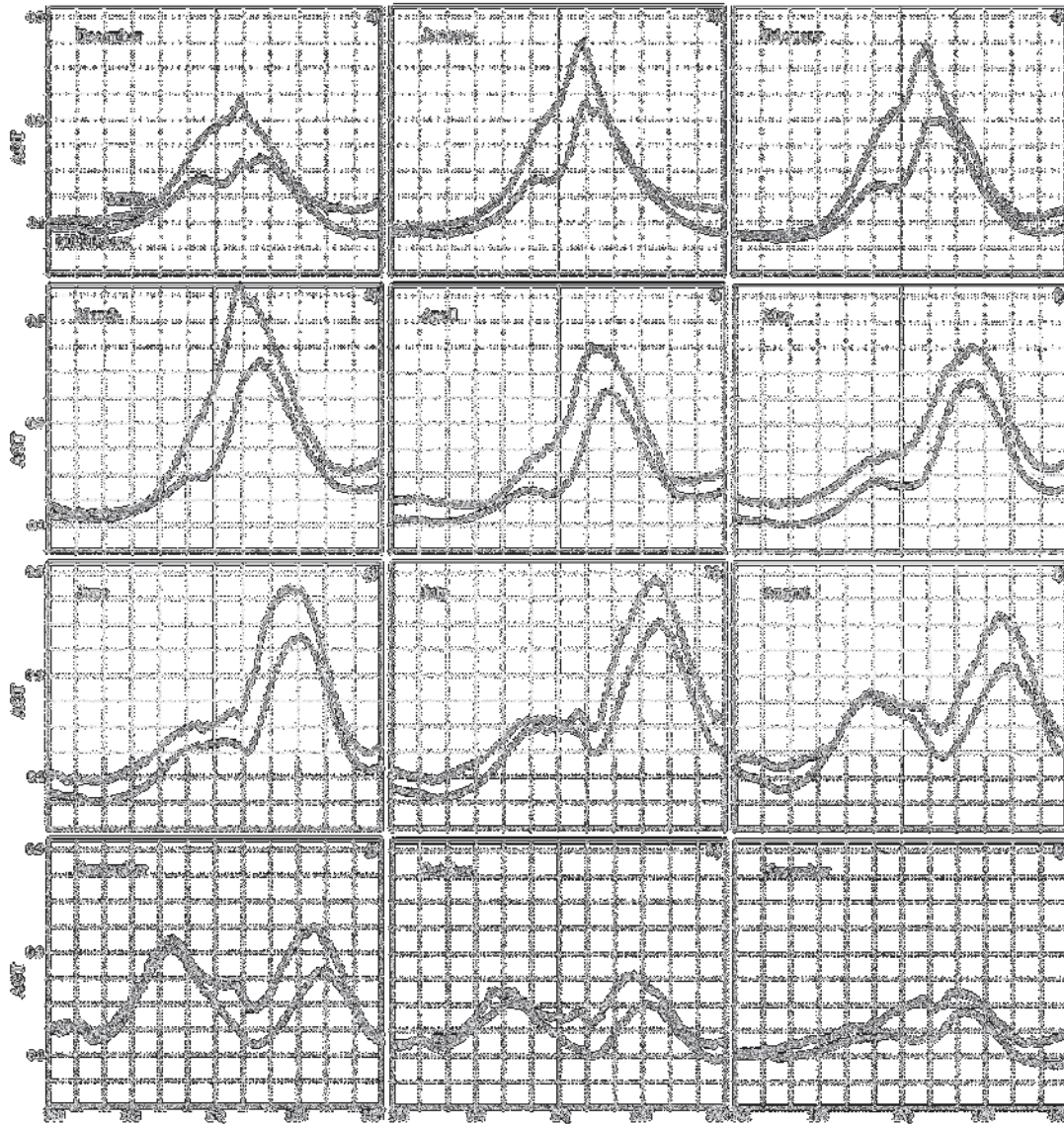
1



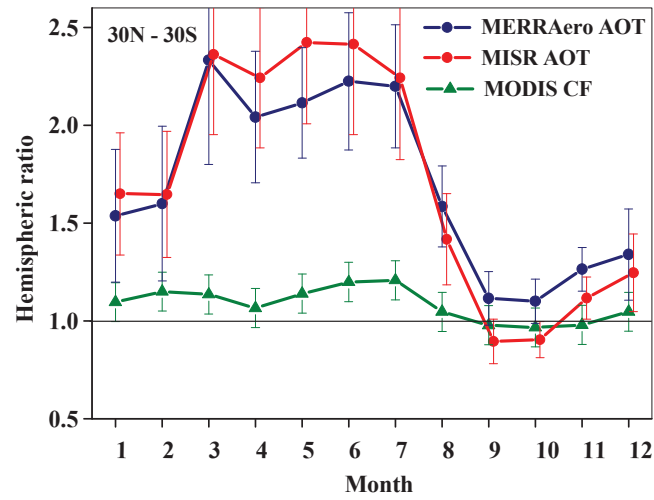
2

3 Figure 2. The meridional distribution of 10-year mean AOT/ CF, zonal averaged over the
4 Atlantic Ocean (60°W – 0°E): a –total AOT based on MERRAero and MISR data; b –
5 MODIS CF, c - MERRAero total AOT, dust AOT (DU), organic and black carbon AOT (OC
6 & BC), and other aerosol species AOT (Other). The vertical lines designate the position of the
7 equator.

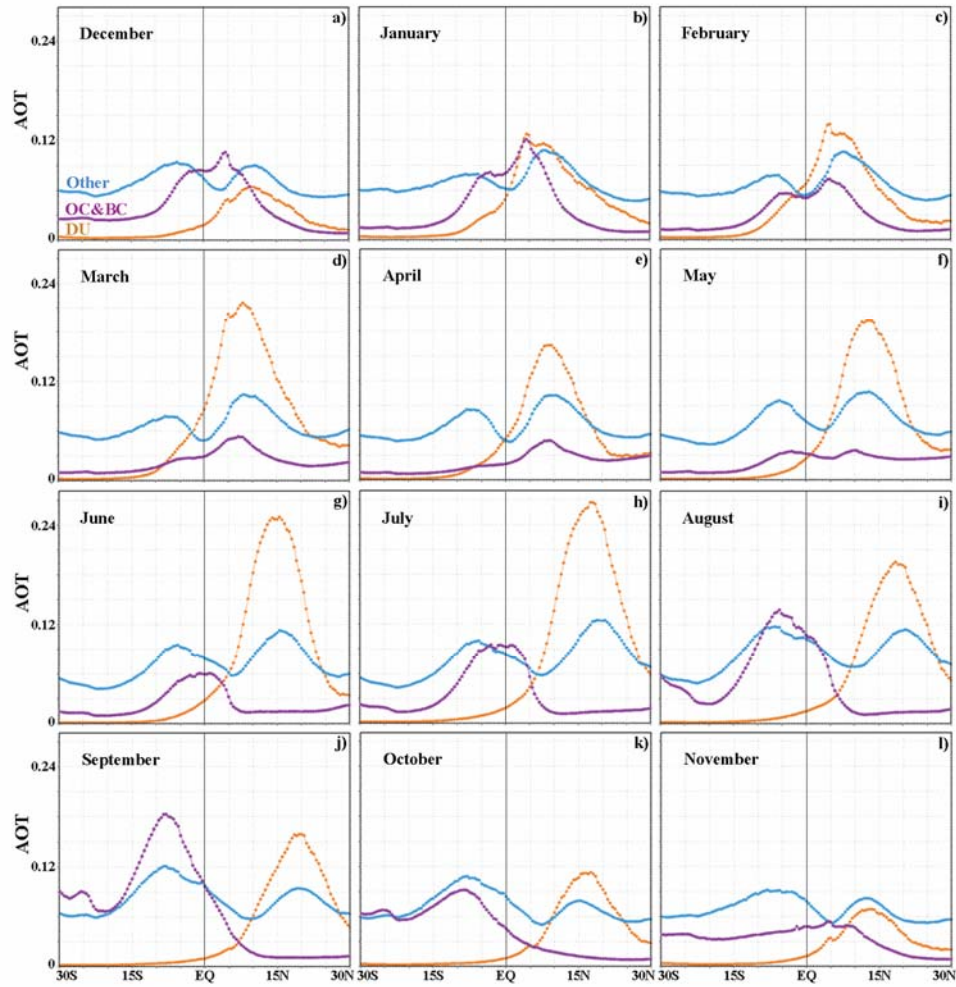
8



1
 2 Figure 3. Meridional distribution of MISR and MERRAero total AOT, zonal averaged over
 3 the Atlantic Ocean, for all months of the year. The vertical lines designate the position of the
 4 equator.
 5



2 Figure 4. Month-to-month variations of the hemispheric ratio (R) of MISR AOT, MERRAero
3 AOT and MODIS cloud fraction (CF) over the tropical Atlantic Ocean (30°N – 30°S). The
4 error bars show the standard deviation of R.
5



2

3

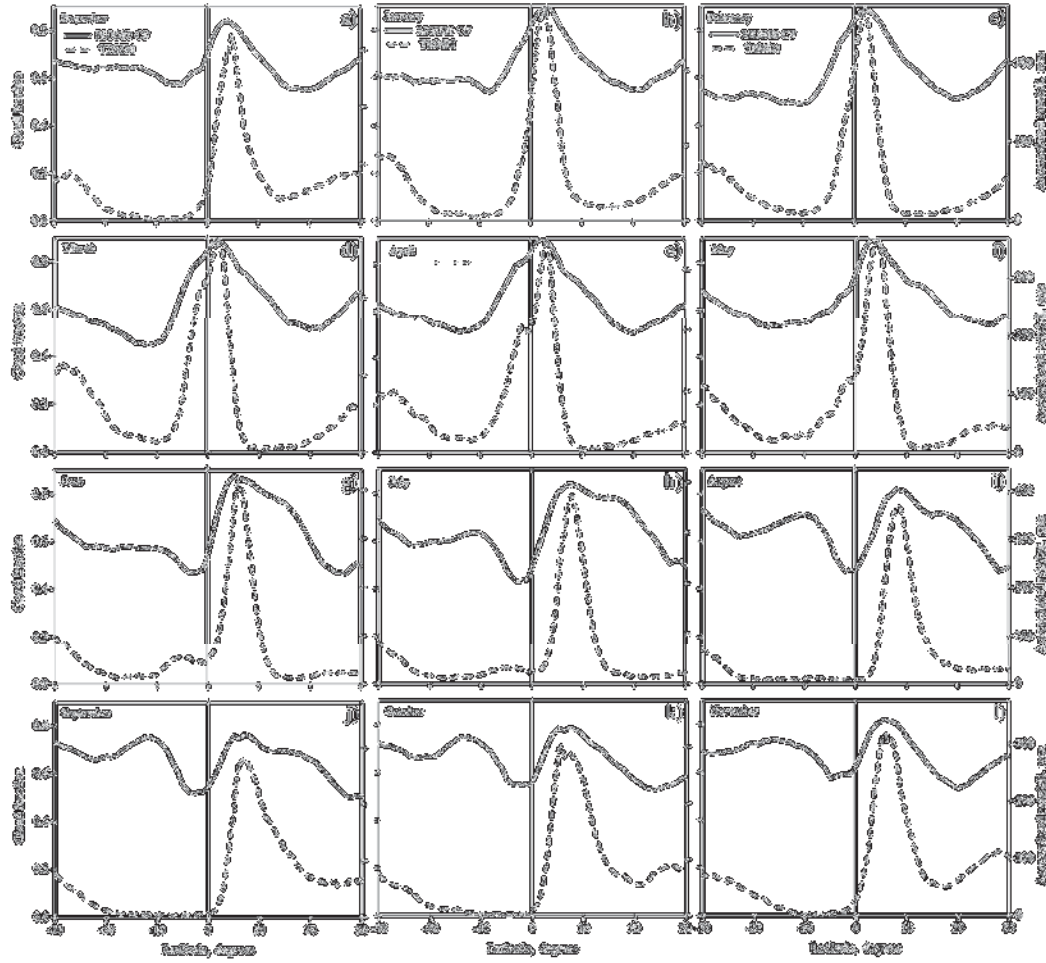
4

5

6

7

Figure 5. Meridional distribution of dust AOT (DU), organic and black carbon aerosol AOT (OC & BC), and other aerosol species AOT (Other), zonal averaged over the Atlantic Ocean, for all months of the year, based on 10-year MERRAero data. The vertical lines designate the position of the equator.

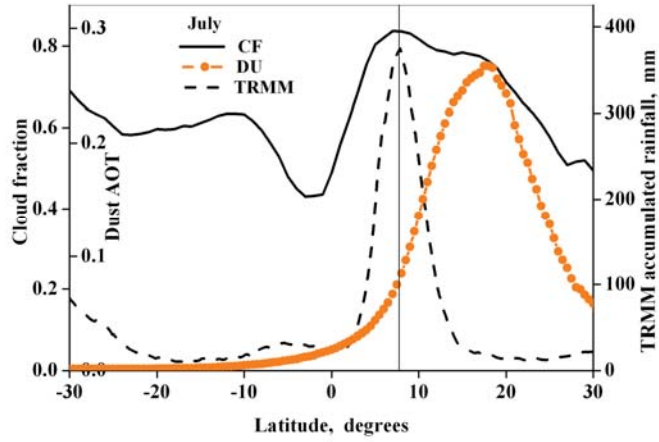


2

3 Figure 6. Meridional distribution of MODIS-Terra CF and TRMM accumulated rainfall,
 4 zonal averaged over the tropical Atlantic Ocean, for all months of the year. The vertical lines
 5 designate the position of the equator.

6

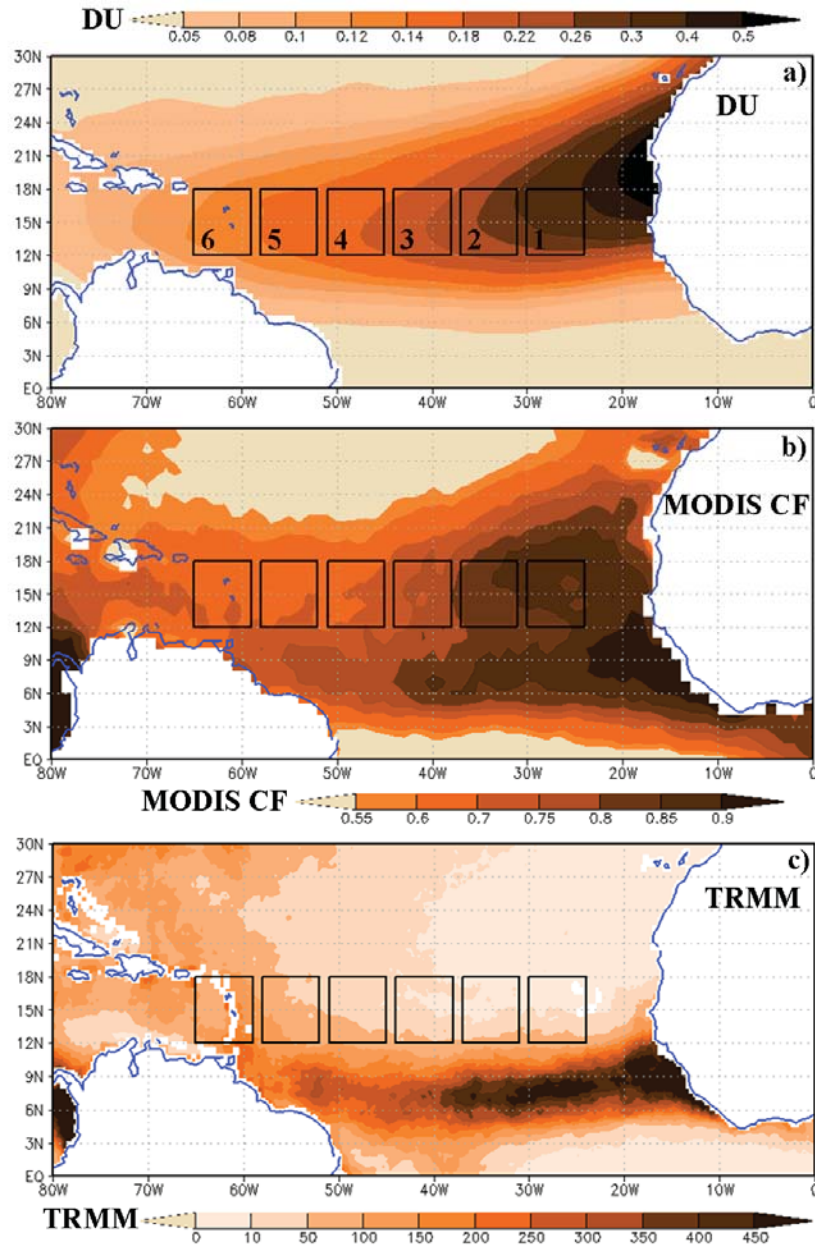
1



2

3 Figure 7. Meridional distribution of 10-year mean MODIS-Terra cloud fraction (CF), TRMM
4 accumulated rainfall and MERRAero dust AOT (DU), zonal averaged over the Atlantic
5 Ocean (60°W – 0°E), in July. The near-equatorial maximum in meridional distribution of
6 TRMM accumulated rainfall indicates the position of the North Atlantic Ocean inter-tropical
7 convergence zone (ITCZ). The vertical lines designate the position of the center of ITCZ.

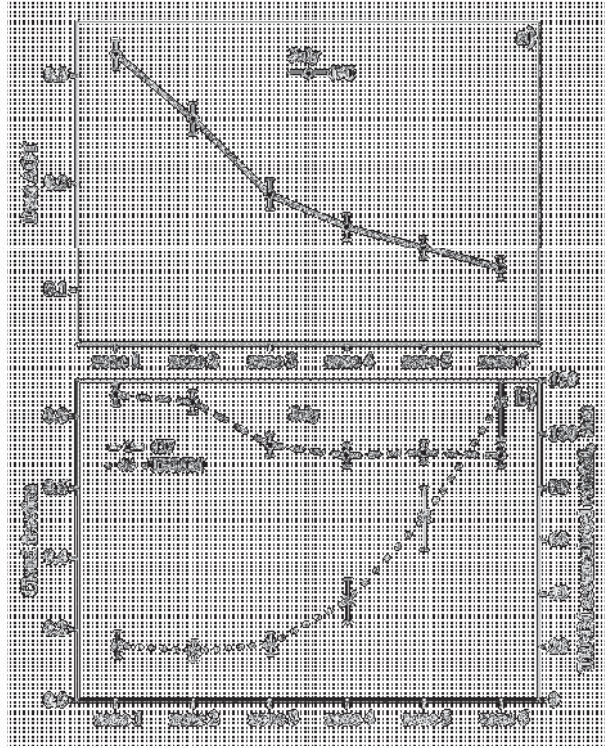
8



2 Figure 8. Spatial distributions of 10-year mean (a) MERRAero dust AOT (DU), (b) MODIS-
 3 Terra CF, and (c) TRMM accumulated rainfall over the North Atlantic in July. The
 4 geographic coordinates of the specified zones are as follows: zone 1 (12°N – 18°N; 30°W –
 5 24°W), zone 2 (12°N – 18°N; 37°W – 31°W), zone 3 (12°N – 18°N; 44°W – 38°W), zone 4
 6 (12°N – 18°N; 51°W – 45°W), zone 5 (12°N – 18°N; 58°W – 52°W), zone 6 (12°N – 18°N;
 7 65°W – 59°W).

8

1



2

3

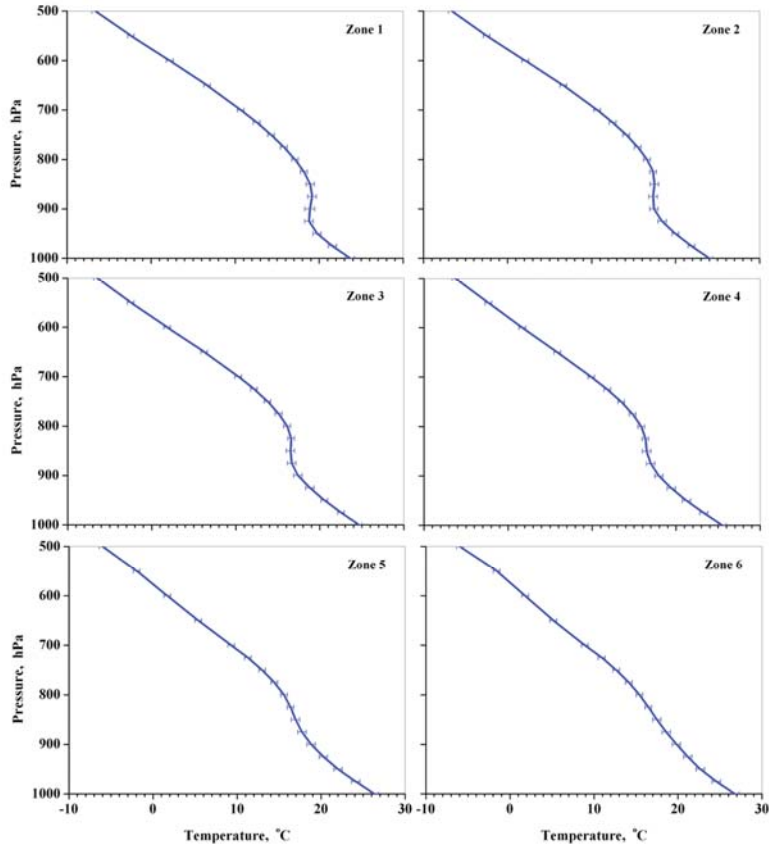
4

5

6

Figure 9. Zone-to-zone variations of (a) MERRAero dust AOT (DU); (b) MODIS-Terra CF and TRMM accumulated rainfall over the specified zones in July, averaged over the ten-year study period (2002 – 2012). The error bars show the standard error of mean.

1



2 Figure 10. Vertical profiles of 10-year mean MERRA atmospheric temperature ($^{\circ}\text{C}$) in July,
3 averaged over the specified zones along the route of transatlantic dust transport. The error
4 bars show the standard deviation of temperature.